Ultralow-Threshold Two-Photon Pumped Amplified Spontaneous Emission and Lasing from Seeded CdSe/CdS Nanorod Heterostructures

Guichuan Xing,[†,¶,§] Yile Liao,[‡,§] Xiangyang Wu,[∥] Sabyasachi Chakrabortty,[‡] Xinfeng Liu,[†] Edwin K. L. Yeow,[∥] Yinthai Chan,[‡,⊥,*] and Tze Chien Sum[†,¶,*]

[†]Division of Physics and Applied Physics, School of Physical and Mathematical Sciences, Nanyang Technological University, 21 Nanyang Link, Singapore 637371, [‡]Department of Chemistry, National University of Singapore, 3 Science Drive 3, Singapore 117543, [⊥]Institute of Materials Research & Engineering, A*STAR, 3 Research Link, Singapore 117602, [∥]Division of Chemistry and Biological Chemistry, School of Physical and Mathematical Sciences, Nanyang Technological University, 21 Nanyang Link, Singapore 637371, and [¶]Energy Research Institute @ NTU (ERI@N), Nanyang Technological University, 50 Nanyang Drive, Singapore 637553

ABSTRACT Ultralow-threshold two-photon pumped amplified spontaneous emission (2ASE) and lasing in seeded CdSe/CdS nanodot/nanorod heterostructures is demonstrated for the first time. Such heterostructures allow the independent tunability of the two-photon absorption (2PA) cross-section (σ_2) through varying the CdS rod size, and that of the emission wavelength through varying the CdSe dot size. With an enhanced σ_2, 2ASE in these heterostructures is achieved with an ultralow threshold fluence of ~1.5 mJ/cm^2, which is as much as one order less than that required for spherical semiconductor NCs. Importantly, by exploiting this unique property of the seeded nanorods exhibiting strong quantum confinement even at relatively large rod sizes, a near reciprocal relation between the 2ASE threshold and the 2PA action cross-section ($\sigma_2\eta$) (where η is the quantum yield) was found and validated over a wide volume range for II–VI semiconductor nanostructures. Ultrafast optical spectroscopy verified that while the Auger processes in these heterostructures are indeed suppressed, ASE in these samples could also be strongly affected by a fast hole-trapping process to the NR surface states. Lastly, to exemplify the potential of these seeded CdSe/CdS nanodot/nanorod heterostructures as a viable gain media for achieving two-photon lasing, a highly photostable microsphere laser with an ultralow pump threshold is showcased.

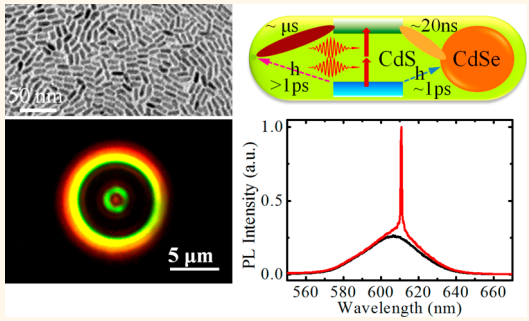

KEYWORDS: CdSe/CdS nanorod · upconversion · whispering gallery mode lasing · two-photon absorption · ultrafast

Colloidal semiconductor nanocrystals (NCs) are desirable as optical gain media due to their excellent photostability, continuous tunability over a wide spectral range, and easy chemical processability.[1−17] These advantageous physicochemical properties make NCs highly suited for optical applications such as multiwavelength on-chip microcavity lasers and as miniaturized light sources in lab-on-a-chip diagnostics.[1−16] To date, optically pumped amplified spontaneous emission (ASE) and lasing in colloidal semiconductor NCs have largely been demonstrated using one-photon excitation (1PE) with ultraviolet/visible light sources.[1−12] However, it is foreseeable that in many of the applications for which NC lasers are relevant the use of UV–vis excitation wavelengths risks the high possibility of photodamage to the sample and substrate or unwanted excitation of fluorescent contaminants present in the application setup. A promising route to the derivation of ASE and lasing in NCs while circumventing the above issues is optical pumping *via* two-photon excitation (2PE) at infrared (IR) wavelengths.[12−16]

2PE is achieved through the simultaneous absorption of two photons, which induces an electronic transition from the ground state to an excited state *via* virtual states. In contrast to 1PE, 2PE possesses several unique features such as higher spatial resolution and longer penetration depth when operating in the semitransparent infrared window of biological media and has

* Address correspondence to tzechien@ntu.edu.sg; chmchany@nus.edu.sg.

Received for review September 12, 2012 and accepted November 16, 2012.

Published online November 17, 2012
10.1021/nn304200a

thus been exploited for bioimaging.[12−16,18−21] Additionally, for the generation and wavelength tuning of coherent light, the absence of a phase matching requirement in the 2PE process makes it highly attractive over other nonlinear frequency conversion techniques (*e.g.*, optical harmonic generation), as this permits its application to a much wider range of resonator designs and gain media (other than birefringent crystalline materials).[12−16] Given the advent of robust, low-cost, versatile, and compact IR laser sources (*e.g.*, fiber lasers), 2PE has become a viable technique for the generation of coherent light *via* the attainment of optical gain in colloidal semiconductor NCs.

One major impediment to the development of practical two-photon pumped colloidal semiconductor NC lasers is the small two-photon absorption (2PA) cross-section (typically $\sigma_2 \approx 10^{-46}$ cm^4/photon) for most spherical core−(thin) shell II−VI semiconductor NCs that necessitate the use of high laser excitation fluences to derive optical gain. Thus, prior efforts to achieve two-photon induced stimulated emisison in NCs typically resulted in very high thresholds of over 10 mJ/cm^2.[12−16] For 2PE, the average number of electron−hole (e−h) pairs created by each laser pulse is given as $\langle N_2 \rangle = f^2\sigma_2/\tau_p$, where f is the fluence and τ_p is the pulse duration. For a fixed τ_p, it is desirable to increase σ_2 and reduce f for the same $\langle N_2 \rangle$ in order to reduce the likelihood of photodamage to the gain media. While simply increasing the volume of strongly confined NCs to increase σ_2 appears to be a straightforward solution, an increase in size for these strongly quantum-confined NCs inevitably red shifts their band-edge fluorescence, thereby imposing severe limitations on their spectral tunability. For the fabrication of devices with wavelength-specific requirements such as lasers, this presents a formidable challenge.

Herein we demonstrate that these issues may be simultaneously addressed using seeded CdSe/CdS nanorod (NR) heterostructures, which comprise a spherical CdSe core that is encapsulated by a rod-like CdS shell as the optical gain media. While the CdS shell functions as an antenna in light harvesting, emission from the rod originates primarily from the quantum-confined CdSe core.[8,22−25] This unique optical configuration thus allows for σ_2 and the emission wavelength to be varied independently by adjusting the physical dimensions of the rod-like shell and spherical core, respectively. We then show that *via* the use of highly monodisperse CdSe-seeded CdS NRs, room-temperature ASE *via* 2PE at 800 nm can be obtained with thresholds as low as 1.5 mJ/cm^2. The NRs were subsequently incorporated into a silica matrix and coupled to a microspherical cavity, where single-mode lasing at a threshold of 0.99 mJ/cm^2 was derived. At such low pump intensities, lasing from the NRs *via* 2PE was stable over the course of 6×10^6 laser shots under ambient conditions, thus making these NC laser devices plausible for use in practical applications. Ultrafast optical spectroscopy (UOS) also revealed that while the nonradiative Auger recombination processes ($\tau_{Auger} \approx 200-300$ ps) are indeed suppressed in these NR heterostructures, the ASE could still be strongly affected by the ultrafast hole trapping to the NR surface.

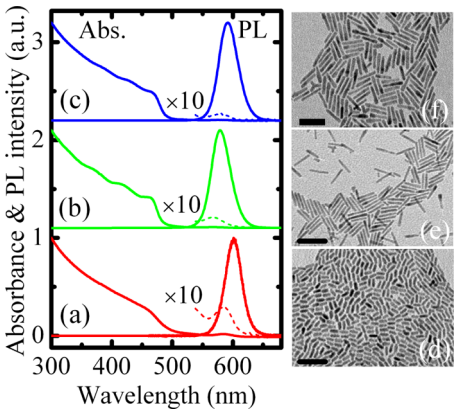

Figure 1. (a−c) Normalized UV−visible absorption spectra (solid line) and its magnified (×10) region (dashed line), 400 nm excited PL spectra for 15, 34, and 39 nm CdSe/CdS nanodot/nanorod heterostructures, respectively. (d−f) Corresponding TEM images; scale bars are 50 nm.

RESULTS AND DISCUSSION

In this work, seeded CdSe/CdS NR heterostructures of three different rod lengths (*i.e.*, 15, 34, and 39 nm) with the same CdSe core (~2.4 nm) were investigated. The size of the CdSe core (<2.8 nm) indicates that these rods are expected to exhibit a quasi-type II core−shell energy profile.[24] The photoluminescence (PL) quantum yield (QY) of these NRs in toluene were measured to be 0.75, 0.61, and 0.56, respectively. Their structure and basic optical properties are shown in Figure 1. These NR samples in toluene were spin casted onto glass slides to form close-packed thin films of NRs, with thicknesses of ~500 nm. The surface roughness of these films was characterized using tapping mode atomic force microscopy, which yielded typical root-mean-square roughness values of ~6 nm measured over a 2 μm × 1 μm scan area.

Optical gain in type-I colloidal semiconductor NCs is generally achieved with the generation of multi-excitons due to the spin degeneracy in its first excited state. For example, due to a 2-fold degeneracy in the $1S_e-1S_h$ transition of CdSe NCs, biexcitons are required in order to derive optical gain.[1,26] The 2PA cross-section σ_2 thus becomes an important metric in determining the photon flux required to generate biexcitons *via* 2PE and subsequently achieve stimulated emission. In the case of ASE from NC-based waveguides, it is fairly obvious that increasing σ_2 without exacerbating other key parameters such as NC volume fraction, Auger recombination rates, and waveguide Q factors would result in lower threshold

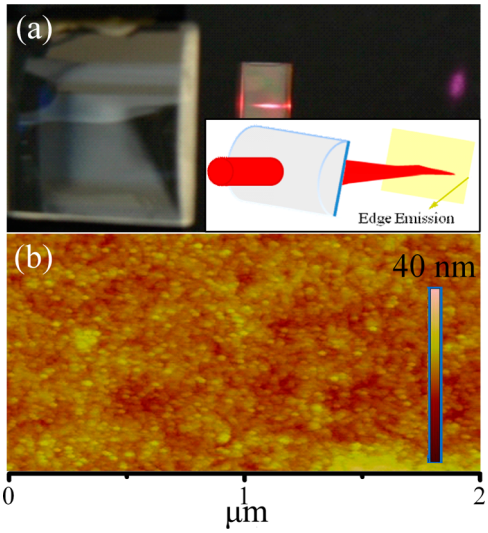

Figure 2. (a) Digital photograph of frequency-upconverted stimulated emission from a CdSe/CdS heterostructure film, pumped by 2PA at 800 nm. Inset shows the pumping configuration. (b) Tapping mode AFM image of the typical surface profile of the close-packed CdSe/CdS heterostructure films.

fluences. The relationship between the PLQY and the ASE threshold, however, can be rather complex. On one hand, the PLQY may not be as important a factor compared to the extremely fast Auger recombination rates if its nonradiative contribution is comparatively slower. On the other hand, the PLQY is a reflection of the degree of passivation of the NC surface, which has been shown by several reports to be strongly related to Auger recombination processes in the NC.[27,28] Furthermore, given that the carriers are generated primarily in the CdS shell and then undergo charge transfer to the CdSe core in these NR heterostructures, carrier trapping processes to the NR surface states can also be a highly efficient nonradiative pathway that competes effectively with both ASE and Auger recombination processes. Finally, the single-exciton PLQY is likely to play a role in the provision of seed photons for the photon cascade that occurs in ASE. Hence, to take into account the contributions from these factors, we use the two-photon action cross-section (*i.e.*, $\sigma_2 \times \eta$) of the NC sample as a basis for analyzing the relationship between the threshold fluence and σ_2.

Determination of 2PA Cross-Sections. As the two-photon-pumped ASE of the NR films is strongly dependent on the nonlinear absorption properties of the CdSe-seeded CdS NRs, we first determined the 2PA cross-sections (σ_2) of these NR heterostructures using the open-aperture Z-scan technique with 150 fs laser pulses (1 kHz) at a wavelength of 800 nm.[20] Table 1 lists the σ_2 values measured for samples with different rod lengths, which can ostensibly be described as exhibiting a superlinear dependence. Elucidating the physical origins of this superlinear dependence is nontrivial, though it is likely due to the local field

TABLE I. Average Length, Quantum Yield (η), 2PA Cross-Section (σ_2), Two-Electron-Hole Pair Decay Time (τ_2), and 2ASE Threshold of CdSe/CdS Nanodot/Nanorod Heterostructures

length (nm)	η [%]	σ_2[a] [GM]	τ_2 [ps]	threshold [mJ/cm^2]
15	75	70 000	190	3.4
34	61	190 000	260	1.8
39	56	230 000	300	1.5

[a] Experimental uncertainty: ±20%.

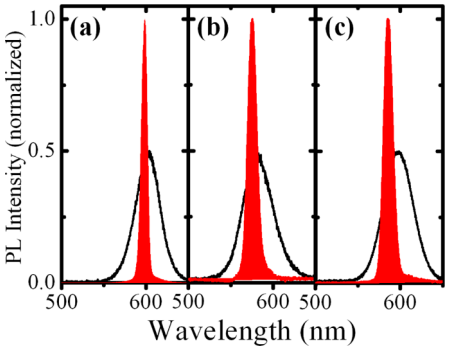

Figure 3. 2ASE spectra (red) obtained from the films with 15 nm (a), 34 nm (b), and 39 nm (c) CdSe/CdS heterostructures at an 800 nm pump wavelength. The 2PA-induced SE spectra (black) are also shown for each corresponding sample.

effects on the nanostructure size and the density of states.[18−20] For 39 nm long NRs, a σ_2 value of 2.3×10^5 GM (where 1 GM = 10^{-50} cm^4 s/photon) was measured, which is 2 to 4 orders of magnitude larger than that previously reported for spherical semiconductor QDs and about 4 orders of magnitude larger than that of typical organic dyes.[18−20] Importantly, σ_2 can be varied independently of the CdSe core, whose size primarily determines the emission wavelength. The advantages of size-dependent emission afforded by the quantum-confined CdSe core are therefore preserved in these heterostructures.

Two-Photon Pumped Amplified Spontaneous Emission. Figure 3a−c show the normalized room-temperature emission spectra below and above the two-photon-pumped ASE (2ASE) threshold for 15, 34, and 39 nm long CdSe-seeded CdS NRs with a CdSe core size of ~2.4 nm, respectively. Following 2PA, which is dominated by the CdS shell, electron−hole pairs are formed and undergo ultrafast charge localization to the CdSe core within ~1 ps, where radiative recombination occurs.[8,25] Below the threshold fluence, the two-photon pumped spontaneous emission (SE) of the heterostructures dominates the light output with a bandwidth of ~40 nm (*i.e.*, full width at half-maximum (fwhm)). These spectra are indistinguishable from the 1PE PL spectra shown in Figure 1. Above this threshold, the emission bandwidth reduced to less than 12 nm for all the samples, as a result of gain-induced narrowing.

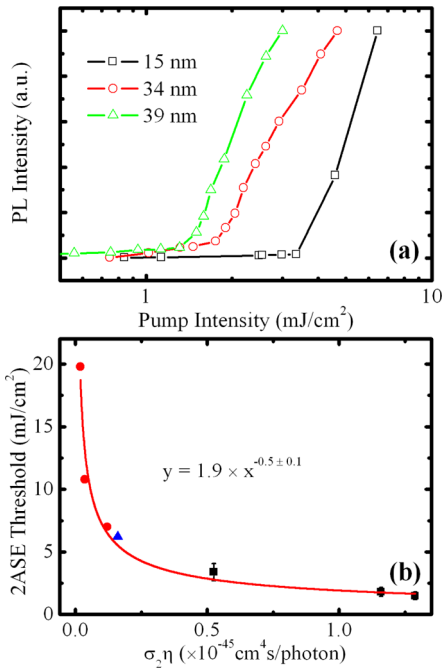

Figure 4. (a) Variable fluence measurements show the 2ASE thresholds of the CdSe/CdS heterostructures. (b) Plot of 2ASE *vs* 2PA action cross-section ($\sigma_2\eta$). The experimental results were taken from present work (■), ref 14 (●), and ref 15 (▲). The red line is a power-law fitting.

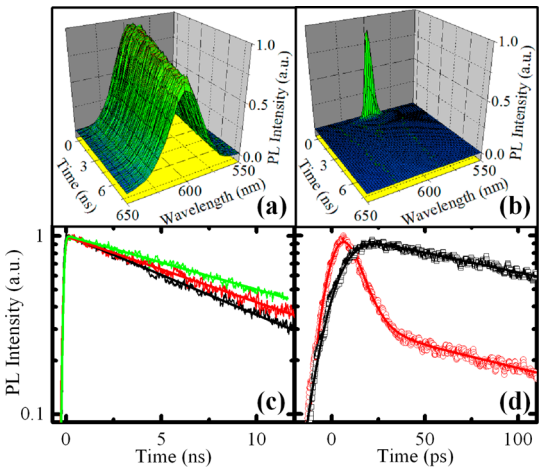

Figure 5. Typical 3D time-resolved 2PA-induced SE (a) and ASE (b) spectra for 15 nm CdSe/CdS heterostructure films. (c) 2PA-induced SE (integrated ±5 nm around the emission peak) decay curves and the single-exponential fittings for 15 nm (black), 34 nm (red), and 39 nm (green) heterostructure films. (d) Typical time-resolved PL traces with 2PA excitation fluence just below (black) and above (red) the ASE threshold for the 15 nm heterostructure film.

Notably, the 2ASE peaks of all the samples are blue-shifted with respect to the exciton peak with energy separations of 10, 29, and 47 meV for the 15, 34, and 39 nm NR heterostructures, respectively. The origins of this blue shift may be attributed to the quasi-type-II band alignment between the CdSe core and CdS shell (valid for CdSe core sizes < 2.8 nm[22−25]), which results in a negative biexciton binding energy (repulsive exciton−exciton interaction) that causes its radiative recombination to occur at a higher energy than that of the single exciton.[1,4,7,26] This repulsive interaction increases with the length of the NR and stems from a decreased overlap of the electron−hole wave functions due to an increased electron wave function delocalization into the rod-like shell. The resulting reduced attractive electron−hole interaction is subsequently commensurate with a stronger repulsive interaction between charges in the core and shell.[1,4,7,26] It should be noted that it is unlikely that single-exciton 2ASE from these heterostructures was obtained since the biexciton repulsion energy is much smaller than the ensemble line width of the single-exciton emission (*i.e.*, ∼130 meV).[7] Within quasi-type-II band alignment of the CdSe/CdS heterostructure, the 2ASE peak should be tunable between ∼550 and ∼600 nm by tailoring the CdSe core and CdS shell size.[11,22,24]

Figure 4a shows the dependence of the integrated PL intensity on the pump fluence. At relatively low pump intensities (*i.e.*, <1.2 mJ/cm^2), the PL emission shows a near quadratic pump intensity dependence for all the samples, which validates the 2PA process at 800 nm.[20,29] At higher pump intensities, an abrupt change of the slope occurs, indicating a threshold behavior that is characteristic of 2ASE. The 2ASE threshold pump intensities for the 15, 34, and 39 nm CdSe/CdS heterostructures were found to be 3.4, 1.8, and 1.5 mJ/cm^2, respectively, for samples with comparable film thicknesses (∼500 nm) and loading fraction (∼30%).[15] It is evident that the 2ASE threshold pump fluence decreases with increasing rod length, which may be attributed to the increased σ_2. The 2ASE threshold pump intensities as a function of the heterostructures' 2PA action cross-section ($\sigma_2\eta$) are presented in Figure 4b. The plot summarizes the experimental results from this study as well as those collated from the literature.[14,15] From the fit, the 2ASE threshold pump intensities exhibit a power-law dependence of -0.5 ± 0.1 to $\sigma_2\eta$. It shows that the 2ASE threshold is nearly inversely proportional to $\sigma_2\eta$ (*i.e.*, a near reciprocal relation), which is consistent with the notion that the enhanced 2PA cross-section at 800 nm due to the CdS rod-like shell would effectively lower the pump intensities needed to achieve ASE. Within our range of samples measured, the 39 nm long CdSe-seeded CdS NRs have the largest 2PA action cross-section and yielded, to the best of our knowledge, the lowest 2ASE threshold to date (*i.e.*, ∼1.5 mJ/cm^2) for a colloidal NC system. Comparatively, this value is as much as 1 order less than that obtained for spherical quantum dots.[14,15] We emphasize that this comparison is based on the achievement of ASE in a waveguide geometry, where unlike in the case of lasing in optical cavities, the thresholds obtained are less strongly dependent on cavity *Q* factors and modal volumes. On the basis of the

2PA cross-sections measured with the Z-scan technique, the number of electron−hole pairs generated per NC at threshold pump fluence are estimated to be approximately 1.3, 1.1, and 1.0 for 15, 34, and 39 nm long CdSe-seeded CdS NRs, respectively. This result is consistent with previous observations that the NR optical gain derives primarily from the generation of biexcitons.[1−16]

Transient Optical Spectroscopy. Time-resolved two-photon excited PL experiments at room temperature were also performed on the NR films in order to investigate the biexciton modal gain dynamics in these heterostructures. Typical time-resolved three-dimensional (3D) plots of the 2PA-induced SE and ASE spectra for the 15 nm CdSe/CdS heterostructures are shown in Figure 5a and b, respectively, while the emission decay curves for all the samples and their corresponding decay fits are shown in Figure 5c (*i.e.*, extracted at the peak of the excitonic emission and photoexcited with a pump fluence of ~0.1 mJ/cm^2). It is readily seen that the time dynamics of 2PA-induced SE are similar to that of 1PE and the intensity decays with time *via* a single-exponential function, with fitted decay lifetimes for the 15, 34, and 39 nm rods at 10, 12, and 14 ns, respectively. These fitted lifetimes show that the exciton PL lifetimes increase with increasing rod length, in accordance with the decrease in the CdSe electron−hole wave function overlap due to more extensive delocalization of the electron wave function in the longer rods. However, compared to an ensemble of relatively isolated NRs in a dilute solution (*i.e.*, in a solvent $-\tau_{solution} \approx 20$ ns), the lifetimes obtained for these close-packed films are slightly shorter, likely due to dipole-mediated energy transfer processes between neighboring rods.[30] The energy transfer time (τ_{ET}) is estimated to be around tens of nanoseconds with $1/\tau_{film} = 1/\tau_{solution} + 1/\tau_{ET}$. Therefore, the dipole−dipole interaction between neighboring rods in our film is not expected to have any significant effect on the 2ASE threshold. (2ASE occurs on a much faster time scale as shown below).

At pump fluences above threshold for the 15 nm rod sample, a short-lived, spectrally narrow emission band emerges at energies higher than that of the 2PA-induced SE peak, as shown in Figure 5b. Figure 5d shows its luminescence decay profile at the peak wavelength of the ASE transition for pump fluences below (*i.e.*, ~3 mJ/cm^2) and above threshold (*i.e.*, ~3.5 mJ/cm^2). It should be noted that at the high pump fluence of ~3 mJ/cm^2 this is already in the regime of multiexciton generation, even though the fluence is just below the threshold needed for ASE. Therefore, the PL decay dynamics exhibit a short lifetime component of ~200 ps, which is much shorter than the typical ~10 ns excitonic recombination lifetimes for these NRs. This 200 ps relaxation time closely matches the Auger-limited biexciton recombination lifetimes in these CdSe/CdS heterostructures, which were probed using ultrafast transient absorption (TA) spectroscopy, and

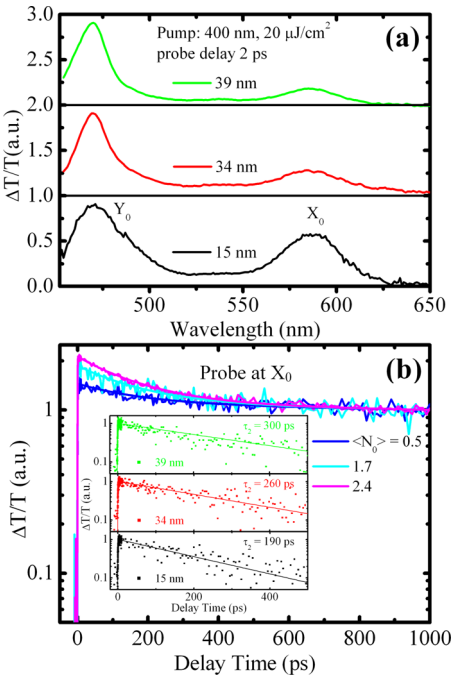

Figure 6. (a) Differential transmission spectra for the nanoheterostructures in toluene solution at a probe delay of 2 ps. The bleaching peaks corresponding to the lowest lying energy levels in CdS and CdSe are labeled Y_0 and X_0, respectively. (b) Pump fluence-dependent decay transients of X_0 normalized to their long-lived decay component for the 15 nm CdSe/CdS nanorods. The inset shows the decay transients of the two electron−hole pair states for the NRs with different lengths, fitted with a single-exponential decay function (line).

these results will be presented in the next paragraph. Beyond the threshold fluence of ~3.5 mJ/cm^2, an even shorter fitted lifetime component of ~7 ps dominates the radiative recombination dynamics, in addition to the ~200 ps Auger-limited biexciton recombination lifetime. This even faster lifetime component is due to the ASE resulting from an avalanche of biexcitonic recombination, where its lifetime measurements are limited by the system temporal response of the streak camera.

Optical gain in semiconductor NCs is strongly dependent on the competition between radiative and nonradiative processes (*i.e.*, multiexciton Auger recombination, fast charge carrier trapping, *etc.*). Therefore, it is very important to elucidate and gain a clear understanding of the dynamic interplay between the various carrier relaxation channels through TA spectroscopy. Figure 6a shows representative differential transmittance (DT) spectra of these CdSe/CdS heterostructures (in toluene) at probe delay of 2 ps following 3.1 eV photoexcitation. The photobleaching (PB) peaks (*i.e.*, $\Delta T/T > 0$) evident in the DT spectra arise from the state filling of the hole states in the CdSe core and the electron states in the CdS shell. These correspond to the lowest lying energy levels in the CdSe and CdS system and are labeled as X_0 and Y_0, respectively.[8,23,25]

With increasing NR length, the amplitude ratio of X_0 to Y_0 decreases, consistent with an increased absorption from the larger rod-like shell. Pump-power dependent bleaching kinetics at X_0 was performed to elucidate the biexciton Auger recombination lifetimes in these NR heterostructures. Figure 6b shows the representative decay transients for the 15 nm NRs for different pump powers (expressed as an average number of electron–hole pairs). Using a procedure previously reported by Klimov *et al.*,[26] the biexciton Auger recombination lifetimes were extracted and are shown in the inset of Figure 6b. These were fitted to be 190, 260, and 300 ps for the 15, 34, and 39 nm rods, respectively, which are much longer than the biexciton lifetime (*i.e.*, ~45 ps) for 2.3 nm CdSe spherical dots.[26] Hence, it may be inferred that the biexcitonic Auger recombination rates are indeed greatly suppressed in these NR heterostructures. The slower rates found in the longer rods are consistent with the decrease in the CdSe electron–hole wave function overlap caused by the more extensive delocalization of the electron wave function in the longer rods. However, compared to CdSe NRs of similar volume, the biexciton Auger rate is slightly faster in these heterostructures. We attribute this to the strong confinement of the holes in the CdSe core (in our heterostructures) and a more weakly confined electron that delocalizes into the CdS shell. Hence, it is understandable that the Auger dynamics in this system of mixed dimensionality are in-between the case of a zero-dimensional quantum dot and that of a one-dimensional quantum rod.[26] Further experimental investigations and theoretical modeling are under way to gain a clearer understanding of the Auger processes that occur in these heterostructures of mixed dimensionalities. In these CdSe/CdS NR heterostructures where the Auger rates are suppressed, the optical gain buildup time compares favorably with the nonradiative Auger processes.

In light of the fact that the suppressed Auger processes may not play a dominant role in the ultrafast multiexciton dynamics of our 2PE-derived ASE from CdSe/CdS NRs, we examined the dynamics of other possible nonradiative processes, in particular ultrafast charge trapping to surface states and their impact on the ASE process. As discussed previously, the relationship between PLQY and the ASE threshold is complicated. If the PLQY is limited by the ultrafast nonradiative surface-trapping processes, it will play a bigger role than previously envisaged for these mixed-dimensionality heterostructures, and this provides a strong justification for our use of $\sigma_2\eta$ as a basis for analyzing the relationship between threshold fluence and σ_2. Furthermore, our ASE threshold measurements show that the 2ASE threshold is nearly inversely proportional to $\sigma_2\eta$ in the CdSe/CdS NR heterostructures, which indicates that the PLQY (dependent on the NR length) is indeed limited by some ultrafast nonradiative processes

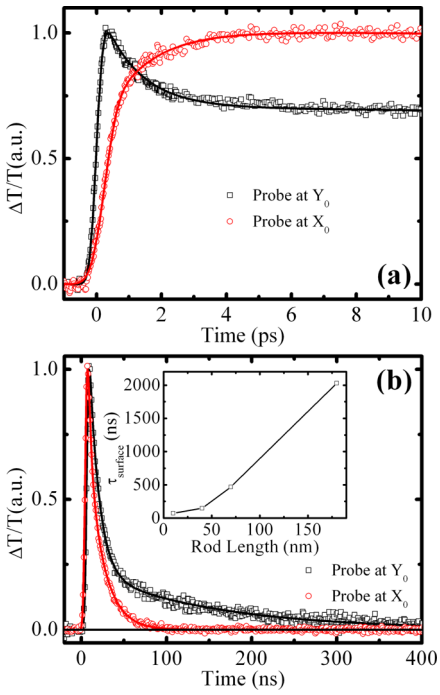

Figure 7. Normalized PB transients at X_0 and Y_0 shown with fs time resolution (a) and ns time resolution (b) for the 39 nm nanorod with an excitation fluence that produces ~1 e–h pair per rod. The inset shows the rod length-dependent surface trapped hole decay lifetime for the heterostructures.

(*i.e.*, other than Auger recombination). The presence of the ultrafast nonradiative surface-trapping processes can be confirmed through TA spectroscopy.

Figure 7a shows the representative normalized bleaching kinetics at X_0 and Y_0 with femtosecond time resolution for the 39 nm NRs upon photoexcitation with a pump fluence of approximately 1 electron–hole (e–h) pair per rod. Following 1PA at 3.1 eV (or 2PA at 1.55 eV), e–h pairs are primarily generated in the CdS shell. This results in an ultrafast buildup of the PB transients (at Y_0) that occurs on a time scale comparable to the pulse width of the femtosecond laser (*i.e.*, ~150 fs). Following fast hole localization from the CdS shell to the CdSe core, the fast buildup of the PB transient at X_0 is simultaneously matched with an equally fast PB decay at Y_0 occurring within 1 ps. The ensuing PL emission originates from the radiative recombination between the strongly localized hole in the core and delocalized electron in the NR shell.[8,22–25] Due to the limitations in temporal resolution (*i.e.*, ~150 fs) of our femtosecond laser and that of the delay line of the fs-TAS setup (*i.e.*, a maximum of ~6 ns, though ~3 ns is typically used), it may be difficult to elucidate the evidence of such surface/trap states from fs-TAS alone. A complementary approach to validating the presence of such nonradiative surface/trap states in the CdS shell would be to examine the recovery of the system back to the equilibrium condition (on a much longer time scale, *i.e.*, tens of ns to μs), with nanosecond (ns-)TA spectroscopy. Figure 7b shows the ns-TA kinetics at Y_0

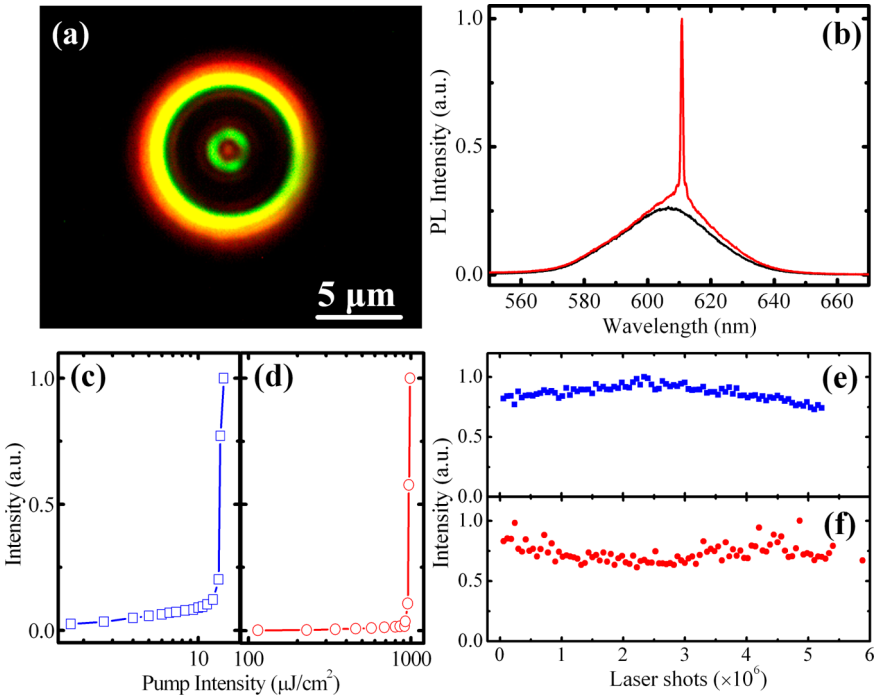

Figure 8. (a) Optical image of a 5 μm silica microsphere coated with a CdSe/CdS NRs silica film. (b) Spectra of a single 5 μm microsphere below (800 μJ/cm^2) and above (990 μJ/cm^2) laser threshold with two-photon pumping. The photoluminescence intensity as a function of pump intensity for one- (blue) (c) and two-photon (red) (d) pumping, respectively. Shot-dependent lasing intensity of a microsphere under one- (e) and two-photon (f) pumping.

and X_0, where the PB dynamics clearly show a prolonged recovery of the PB signals back to the equilibrium for Y_0 (*i.e.*, CdS shell), while those of X_0 have already decayed. The lifetime of the fast PB decay component for both Y_0 and X_0 coincides with the PL lifetime of the heterostructures in toluene. Hence, we attribute this long PB lifetime in Y_0 to arise from the nonrecovery of the electrons in the lowest CdS energy levels back to the equilibrium. This can be attributed to the presence of some holes still being trapped at the CdS surface states. Considering the high PLQY for these heterostructures (*i.e.*, > 50%), we can further infer that the trapping to these surface hole states would have occurred on a time scale slightly longer than the hole relaxing to the CdSe core (*i.e.*, within a few ps), which is comparable to surface hole-trapping lifetimes reported in the literature for other NCs and NRs.[31−33] This assignment is consistent with the rod length-dependent PLQY measurements, where the PLQY decreases with increasing rod length. The longer the NR, the higher the possibility of the holes being trapped at the surface states as they migrate to the CdSe core. The long decay of Y_0 represents the slow recombination between the surface-localized holes with delocalized electrons in the NR. Due to the reduced wave function overlap between localized hole and the delocalized electron in the longer NR, one would expect that the recombination lifetimes would increase as the NR length increases. This is indeed validated by the results in the inset of Figure 7b. Nevertheless, despite that the fast surface hole-trapping time is comparable with the time scales of the biexcitonic recombination avalanche that triggers the ASE, low ASE thresholds can still be achieved due to the large cross-sections and high PLQY (*i.e.*, action cross-sections) of these NR heterostructures.

Lasing from a Spherical Cavity. We demonstrate the potential of these CdSe/CdS NRs as a gain medium for two-photon pumped lasing using a spherical optical cavity. Such optical cavities can potentially possess extremely high *Q* factors because of the strong confinement of photons within a given modal volume.[34,35] The CdSe/CdS NRs described above were chemically functionalized and incorporated into a sol−gel-derived silica matrix to permit the adhesion of a thin layer of NRs-silica onto the exterior of commercially available silica microspheres (with a diameter of 5.0 ± 0.3 μm). The motivation to put NRs−silica composites over a silica sphere instead of NRs directly attached to spheres is to increase the damage tolerance of samples to continuous pulsed excitation. Figure 8a shows an optical image of a typical NR-coated microsphere under optical excitation. Under two-photon (800 nm) pumping, single-mode threshold lasing from the NR-coated microsphere was achieved as shown in Figure 8b. The laser line exhibits a fwhm of ~0.75 nm with a *Q* factor of ~800 (*i.e.*, the *Q* factor is defined as $\lambda/\Delta\lambda$, where λ and $\Delta\lambda$ are the wavelength and the fwhm of the laser emission). This value is

consistent with previously reported values in similar cavities under one-photon pumping[6] and may be attributed to the self-absorption of NRs, scattering from structural defects within the film and surface roughness. Figure 8c and d show the threshold behavior for two-photon pumped lasing in comparison to one-photon pumped lasing. The threshold fluences are 910 ± 50 and 12 ± 2 μJ/cm^2 for two-photon and one-photon pumped lasing, respectively. The ratio of their threshold fluence is ~100, which is typical of those for two-photon to one-photon pumped lasing.[12−16] While slightly lower 2PA lasing thresholds for NCs in spherical optical resonators have previously been reported,[16] it should be recognized that such thresholds are a strong function of the cavity *Q* factor, which is likely to differ significantly from our setup. It should be noted that increasing the size of the NR shell increases not only σ_2 but also that of the one-photon absorption cross-section. Nonetheless, compared to spherical semiconductor QDs under similar experimental conditions, both the one-photon and two-photon pumped lasing thresholds are dramatically lowered in these NRs.[12−16] Lastly, the photostability of our prototype microsphere laser was evaluated by monitoring the lasing intensity as a function of time under a continuous irradiation at a 1 kHz repetition rate under ambient conditions. Figure 8e and f show the variation in lasing intensity over 5×10^6 laser shots under one-photon and two-photon pumping, respectively. Following such a large number of laser pulse excitation events, the near invariance of the output intensity for both cases bears testimony to the excellent optical stability of the microsphere laser with the CdSe/CdS nanodot/nanorod heterostructures as gain media.

CONCLUSIONS

In summary, ultralow-threshold two-photon pumped ASE and lasing with CdSe/CdS nanodot/nanorod heterostructures was demonstrated for the first time. Essentially, these NR heterostructures afford us the means to independently tune the 2PA cross-section using the CdS shell and the quantum-confined emission wavelengths using the CdSe core. Using these NRs as the gain media, the greatly enhanced σ_2 allows us to achieve 2ASE in thin film samples with an ultralow threshold pump fluence of 1.5 mJ/cm^2 for the 39 nm NRs, which is as much as one order less than that needed for 2ASE of spherical quantum dots. Importantly, by exploiting the unique property of the seeded NRs to exhibit strong quantum confinement even at relatively large rod sizes, a near inverse proportional dependence of the 2ASE threshold on the $\sigma_2\eta$ was found and validated over a wide volume range for II−VI semiconductor nanostructures. New insight into the charge dynamics of these NR heterostructures was also uncovered through UOS techniques. Our investigations revealed that while the 2ASE ($\tau \leq 7$ ps) can effectively compete with the suppressed Auger process ($\tau_{Auger} \approx 200$ ps) in these NR heterostructures, the 2ASE could be strongly affected by the competition between hole localization to the CdSe core ($\tau \approx 1$ ps) and to CdS surface states ($\tau > 1$ ps). Lastly, to demonstrate the potential of these NR heterostructures as a viable gain media for achieving 2PE lasing, a high stability prototypical microsphere laser with ultralow pump threshold was showcased.

EXPERIMENTAL SECTION

Seeded CdSe/CdS NRs heterostructures of different rod lengths were prepared according to a previously published procedure[22] with slight modifications. Briefly, spherical CdSe cores of ~2.4 nm in size were first synthesized *via* the hot injection method as described in ref 23 followed by seeded growth of the CdS rod-like shell of different lengths at ~360 °C.

For femtosecond optical spectroscopy, the laser source was a Coherent Legend regenerative amplifier (150 fs, 1 kHz, 800 nm) that was seeded by a Coherent Mira oscillator (100 fs, 80 MHz). Laser pulses of 800 nm wavelength were from the regenerative amplifier's output, while 400 nm wavelength laser pulses were frequency doubled with a BBO crystal.

For Z-scan measurements, the incident laser pulses were focused onto the sample by a lens with 30 cm focal length. The NR heterostructures in toluene solution were placed in a 2 mm thick quartz cell, which was traversed across the focal point along the beam propagation axis.

For femtosecond TA experiments, the samples were pumped at 3.1 eV and probed with a white-light continuum. The probe pulses (400−750 nm) were generated by focusing a small portion (~5 μJ) of the fundamental 800 nm laser pulses into a 1 mm thick sapphire plate. The linear polarization of the pump pulse was adjusted to be perpendicular to that of the probe pulse with a polarizer and a half-wave plate. The cross-polarization will help eliminate any contribution from coherent artifacts at early times. Pump-induced changes of transmission ($\Delta T/T$) of the probe beam were monitored using a monochromator/PMT configuration with lock-in detection. The pump beam was chopped at 83 Hz, and this was used as the reference frequency for the lock-in amplifier.

For 2ASE experiments, the 800 nm laser pulses were focused by a cylindrical lens (with focal length $f = 20$ cm) to a stripe (of dimensions ~0.1 mm × 6 mm) on the films coated on the sample slides, which were aligned perpendicular to the excitation stripe. The emission from the film edge was collected in a lateral configuration by a pair of lenses focused onto an optical fiber coupled to a spectrometer (Acton, Spectra Pro 2500i) and detected by a charge-coupled device (Princeton Instruments, PIXIS 400B CCD).

The two-photon pumped time-resolved PL was detected by an Optronis Optoscope streak camera system, which has an ultimate temporal resolution of ~6 ps when operated at the shortest time window of 330 ps. Lastly, lasing from a single microsphere was observed using a home-built confocal microscope with both the excitation pulses and emission light being coupled and collected through the same long working distance 50× microscope objective (NA = 0.55) and spectrally resolved by the above-mentioned spectrometer and CCD detector.

For nanosecond TA experiments, a laser flash photolysis spectrometer (LKS.60, Applied Photophysics), equipped with a Q-switched Nd:YAG laser (Brilliant B, Quantel), a 150 W pulsed Xe lamp, and a R928 photomultiplier, was used to record nanosecond-difference absorption spectra. Samples were excited

at 440 nm, and each time-resolved trace was acquired by averaging 10 laser shots at a repetition rate of 1 Hz.

Conflict of Interest: The authors declare no competing financial interest. [§]These authors contributed equally to this work.

Acknowledgment. Financial support from NTU start-up grant M58110068, SPMS collaborative Research Award M58110090, NUS start-up grant WBS-R143-000-367-133, A*STAR TSRP grant R143-000-435-305, and DSTA grant R143-000-423-422 is gratefully acknowledged. G.X., X.L., Y.C., and T.C.S. acknowledge the financial support by the Singapore National Research Foundation (NRF) through the Singapore-Berkeley Research Initiative for Sustainable Energy (SinBeRISE) CREATE Programme. X.L. and T.C.S. also acknowledge the financial support by NRF through the Competitive Research Programme under Project No. NRF-CRP5-2009-04.

REFERENCES AND NOTES

1. Klimov, V. I.; Mikhailovsky, A. A.; Xu, S.; Malko, A.; Hollingsworth, J. A.; Leatherdate, C. A.; Eisler, H.-J.; Bawendi, M. G. Optical Gain and Stimulated Emission in Nanocrystal Quantum Dots. *Science* **2000**, *290*, 314–317.
2. Sundar, V. C.; Eisler, H.-J.; Bawendi, M. G. Room-Temperature, Tunable Gain Media from Novel II-VI Nanocrystal-Titania Composite Matrices. *Adv. Mater.* **2002**, *14*, 739–743.
3. Sundar, V. C.; Eisler, H.-J.; Deng, T.; Chan, Y.; Thomas, E. L.; Bawendi, M. G. Soft-Lithographically Embossed Multilayered Distributed-Feedback Nanocrystal Lasers. *Adv. Mater.* **2004**, *16*, 2137–2141.
4. Ivanov, S. A.; Nanda, J.; Piryatinski, A.; Achermann, M.; Balet, L. P.; Bezel, I. V.; Anikeeva, P. O.; Tretiak, S.; Klimov, V. I. Light Amplification Using Inverted Core/Shell Nanocrystals: Towards Lasing in the Single-Exciton Regime. *J. Phys. Chem. B* **2004**, *108*, 10625–10630.
5. Chan, Y.; Steckel, J. S.; Snee, P. T.; Caruge, J. -M.; Hodgkiss, J. M.; Nocera, D. G.; Bawendi, M. G. Blue Semiconductor Nanocrystal Laser. *Appl. Phys. Lett.* **2005**, *86*, 1/073102–3/073102.
6. Snee, P. T.; Chan, Y.; Nocera, D. G.; Bawendi, M. G. Whispering-Gallery-Mode Lasing from a Semiconductor Nanocrystal/Microsphere Resonator Composite. *Adv. Mater.* **2005**, *17*, 1131–1136.
7. Klimov, V. I.; Ivanov, S. A.; Nanda, J.; Achermann, M.; Bezel, I.; McGuire, J. A.; Piryatinski, A. Single-Exciton Optical Gain in Semiconductor Nanocrystals. *Nature* **2007**, *447*, 441–446.
8. Zavelani-Rossi, M.; Lupo, M. G.; Krahne, R.; Manna, L.; Lanzani, G. Lasing in Self-Assembled Microcavities of CdSe/CdS Core/Shell Colloidal Quantum Rods. *Nanoscale* **2010**, *2*, 931–935.
9. Dang, C.; Lee, J.; Breen, C.; Steckel, J. S.; Coe-Sullivan, S.; Nurmikko, A. Red, Green and Blue Lasing Enabled by Single-Exciton Gain in Colloidal Quantum Dot Films. *Nat. Nanotechnol.* **2012**, *7*, 335–339.
10. Cooney, R. R.; Sewall, S. L.; Sagar, D. M.; Kambhampati, P. Gain Control in Semiconductor Quantum Dots *via* State-Resolved Optical Pumping. *Phys. Rev. Lett.* **2009**, *102*, 1/127404–4/127404.
11. Moreels, I.; Rainò, G.; Gomes, R.; Hens, Z.; Stöferle, T.; Mahrt, R. F. Nearly Temperature-Independent Threshold for Amplified Spontaneous Emission in Colloidal CdSe/CdS Quantum Dot-in-Rods. *Adv. Mater.* **2012**, *24*, OP231–5.
12. Todescato, F.; Fortunati, I.; Gardin, S.; Garbin, E.; Collini, E.; Bozio, R.; Jasieniak, J. J.; Guistina, G. D.; Brusatin, G.; Toffanin, S.; *et al.* Soft-Lithographed Up-Converted Distributed Feedback Visible Lasers Based on CdSe-CdZnS-ZnS Quantum Dots. *Adv. Funct. Mater.* **2012**, *22*, 337–344.
13. Oohata, G.; Kagotani, Y.; Miyajima, K.; Ashida, M.; Saito, S.; Edamatsu, K.; Itoh, T. Stable Biexcitonic Lasing of CuCl Quantum Dots under Two-Photon Resonant Excitation. *Phys. E (Amsterdam, Neth.)* **2005**, *26*, 347–350.
14. Jasieniak, J. J.; Fortunati, I.; Gardin, S.; Signorini, R.; Bozio, R.; Martucci, A.; Mulvaney, P. Highly Efficient Amplified Stimulated Emission from CdSe-CdS-ZnS Quantum Dot Doped Waveguides with Two-Photon Infrared Optical Pumping. *Adv. Mater.* **2008**, *20*, 69–73.
15. Zhang, C.; Zhang, F.; Zhu, T.; Cheng, A.; Xu, J.; Zhang, Q.; Mohney, S. E.; Henderson, R. H.; Wang, Y. A. Two-Photon-Pumped Lasing from Colloidal Nanocrystal Quantum Dots. *Opt. Lett.* **2008**, *33*, 2437–2439.
16. Zhang, C.; Zhang, F.; Cheng, A.; Kimball, B.; Wang, A. Y.; Xu, J. Frequency Upconverted Lasing of Nanocrystal Quantum Dots in Microbeads. *Appl. Phys. Lett.* **2009**, *95*, 1/183109–3/183109.
17. Wiersma, D. S. The Physics and Applications of Random Lasers. *Nat. Phys.* **2008**, *4*, 359–367.
18. Pu, S. C.; Yang, M. J.; Hsu, C. C.; Lai, C. W.; Hsieh, C. C.; Lin, S. H.; Cheng, Y. M.; Chou, P. T. The Empirical Correlation between Size and Two-Photon Absorption Cross Section of CdSe and CdTe Quantum Dots. *Small* **2006**, *2*, 1308–1313.
19. He, G. S.; Yong, K. T.; Zheng, Q. D.; Sahoo, Y.; Baev, A.; Ryasnyanskiy, A. I.; Prasad, P. N. Multi-Photon Excitation Properties of CdSe Quantum Dots Solutions and Optical Limiting Behavior in Infrared Range. *Opt. Express* **2007**, *15*, 12818–12833.
20. Xing, G.; Chakrabortty, S.; Chou, K. L.; Mishra, N.; Huan, C. H. A.; Chan, Y.; Sum, T. C. Enhanced Tunability of the Multiphoton Absorption Cross-Section in Seeded CdSe/CdS Nanorod Heterostructures. *Appl. Phys. Lett.* **2010**, *97*, 1/061112–3/061112.
21. He, G. S.; Markowicz, P. P.; Lin, T. C.; Prasad, P. N. Observation of Stimulated Emission by Direct Three-Photon Excitation. *Nature* **2002**, *415*, 767–770.
22. Carbone, L.; Nobile, C.; Giorgi, M. D.; Sala, F. D.; Morello, G.; Pompa, P.; Hytch, M.; Snoeck, E.; Fiore, A.; Franchini, I. R.; *et al.* Synthesis and Micrometer-Scale Assembly of Colloidal CdSe/CdS Nanorods Prepared by a Seeded Growth Approach. *Nano Lett.* **2007**, *7*, 2942–2950.
23. Deka, S.; Quarta, A.; Lupo, M. G.; Falqui, A.; Boninelli, S.; Giannini, C.; Morello, G.; Giorgi, M. D.; Lanzani, G.; Spinella, C.; *et al.* CdSe/CdS/ZnS Double Shell Nanorods with High Photoluminescence Efficiency and Their Exploitation As Biolabeling Probes. *J. Am. Chem. Soc.* **2009**, *131*, 2948–2958.
24. Sitt, A.; Sala, F. D.; Menagen, G.; Banin, U. Multiexciton Engineering in Seeded Core/Shell Nanorods: Transfer from Type-I to Quasi-Type-II Regimes. *Nano Lett.* **2009**, *9*, 3470–3476.
25. Lupo, M. G.; Sala, F. D.; Carbone, L.; Zavelani-Rossi, M.; Fiore, A.; Lüer, L.; Polli, D.; Cingolani, R.; Manna, L.; Lanzani, G. Ultrafast Electron-Hole Dynamics in Core/Shell CdSe/CdS Dot/Rod Nanocrystals. *Nano Lett.* **2008**, *8*, 4582–4587.
26. Klimov, V. I. Spectral and Dynamical Properties of Multiexcitons in Semiconductor Nanocrystals. *Annu. Rev. Phys. Chem.* **2007**, *58*, 635–673.
27. Beard, M. C.; Midgett, A. G.; Law, M.; Semonin, O. E.; Ellingson, R. J.; Nozik, A. J. Variations in the Quantum Efficiency of Multiple Exciton Generation for a Series of Chemically Treated PbSe Nanocrystal Films. *Nano Lett.* **2009**, *9*, 836–845.
28. Talapin, D. V.; Lee, J. S.; Kovalenko, M. V.; Shevchenko, E. V. Prospects of Colloidal Nanoscrystals for Electronic and Optoelectronic Applications. *Chem. Rev.* **2010**, *110*, 389–458.
29. Xing, G.; Ji, W.; Zheng, Y.; Ying, J. Y. Two- and Three-Photon Absorption of Semiconductor Quantum Dots in the Vicinity of Half of Lowest Exciton Energy. *Appl. Phys. Lett.* **2008**, *93*, 1/241114–3/241114.
30. Crooker, S. A.; Hollingsworth, J. A.; Tretiak, S.; Klimov, V. I. Spectrally Resolved Dynamics of Energy Transfer in Quantum-Dot Assemblies: Towards Engineered Energy Flows in Artificial Materials. *Phys. Rev. Lett.* **2002**, *89*, 1/186802–4/186802.
31. Lo, S. S.; Major, T. A.; Petchsang, N.; Huang, L. B.; Kuno, M. K.; Hartland, G. V. Charge Carrier Trapping and Acoustic Phonon Modes in Single CdTe Nanowires. *ACS Nano* **2012**, *6*, 5274–5282.

32. Yan, Y.; Chen, G.; Van Patten, P. G. Ultrafast Exciton Dynamics in CdTe Nanocrystals and Core/Shell CdTe/CdS Nanocrystals. *J. Phys. Chem. C* **2011**, *115*, 22717–22728.
33. Sewall, S. L.; Cooney, R. R.; Anderson, K. E. H.; Dias, E. A.; Sagar, D. M.; Kambhampati, P. State-Resolved Studies of Biexcitons and Surface Trapping Dynamics in Semiconductor Quantum Dots. *J. Chem. Phys.* **2008**, *129*, 1/084701–8/084701.
34. Spillane, S. M.; Kippenberg, T. J.; Vahala, K. J. Ultralow-Threshold Raman Laser Using a Spherical Dielectric Microcavity. *Nature* **2002**, *415*, 621–623.
35. Armani, D. K.; Kippenberg, T. J.; Spillane, S. M.; Vahala, K. J. Ultra-High-Q Toroid Microcavity on a Chip. *Nature* **2003**, *421*, 925–928.